2023

The effects of point mutations at belt-sulfur sites on nitrogenase catalysis

BOSTON UNIVERSITY

ARAM V. CHOBANIAN & EDWARD AVEDISIAN SCHOOL OF MEDICINE

Thesis

THE EFFECTS OF POINT MUTATIONS AT BELT-SULFUR SITES ON NITROGENASE CATALYSIS

by

TIANMEIYUE FAN

B.S., University of Washington Seattle, 2021

Submitted in partial fulfillment of the

requirements for the degree of

Master of Science

2023

Approved by

First Reader

Aaron W. Young, Ph.D.
Assistant Professor of Pharmacology, Physiology and Biophysics

Second Reader

Yilin Hu, Ph.D.
Professor of Molecular Biology and Biochemistry

ACKNOWLEDGMENTS

I would like to express my sincere gratitude to my mentors, Professor Yilin Hu and Professor Markus Ribbe, for their guidance and support throughout my research. Their invaluable insights, expertise, and patience have helped me navigate through the challenges of this project.

I would also like to thank Scientist Chi Chung Lee for his guidance. Your expertise has been instrumental in shaping my thinking and approach to this project.

Additionally, I would like to thank my fellow lab mates Yiling Liu and Mario Grosch for their assistance throughout the research process. Your mentorship, training, and words of encouragement have been invaluable in helping me familiarize and complete this project. Your feedback has been crucial in helping me to refine my ideas and approach.

Finally, I would like to thank my family and friends for their unwavering support and encouragement throughout my academic journey. Your love, encouragement, and understanding have been the foundation of my success.

In conclusion, I am grateful to everyone who has contributed to this project and helped me along the way. Your support and guidance have been invaluable, and I am deeply appreciative of your efforts. Thank you so much!

THE EFFECTS OF POINT MUTATIONS AT BELT-SULFUR SITES ON NITROGENASE CATALYSIS

TIANMEIYUE FAN

ABSTRACT

Background: Although the current understanding proves that dinitrogen reduction occurs at NifDK protein's M-cluster, the exact reduction mechanism remains controversial and is under active research. Recent crystallographic studies from our laboratory have suggested an asymmetric displacement of belt sulfurs of the M-cluster by three dinitrogen species that possibly represent different reduction states of N_2. The current theory proposed by my colleagues is that substrate catalysis occurs through a belt-sulfur mobilization mechanism (Hu, 2022). The three sulfur sites are situated in the center of M-clusters, and they are named S2B, S3A, and S5A. As the substrate-bound clusters rotate through the three belt-sulfur sites in the order of S3A, S2B, and S5A, stepwise substrate reduction takes place, with the S5A site serving as the exit point for reduced products.

Objective: Our lab is interested in the intricate mechanism of enzymatic substrate reduction. With the crystallographic evidence of asymmetrical belt-sulfur displacements during substrate turnover, this research project aims to test the catalytic ability of the nitrogenase enzyme when the three belt-sulfur sites are altered by site-directed mutagenesis.

Methods: Eight sets of *Azotobacter vinelandii nifDK* genes (encoding the catalytic NifDK component of nitrogenase) with various point mutations at belt-sulfur sites were

each transformed into *E. coli*, followed by cell growth and heterologous expression of each NifDK variant. NifDK variant proteins were then isolated, purified, and analyzed. A series of analytical assays were conducted to test for the formation of NifDK components, iron contents in M-cluster, and the ability to perform substrate reduction.

Results: All NifDK mutants, except YM532 and YM533, showed no acetylene reduction activity. YM532 and YM533 showed some, but significantly low acetylene reduction activity. In addition, YM533 showed further reduction from ethylene to ethane. As expected, all eight mutants are cofactor-deficient but contained P-clusters; however, the P-cluster contents of all mutants, as reflected by the presence of less iron atoms, were lower than that of the positive control.

Conclusions: Mutations to belt-sulfur sites led to completely abolished or significantly diminished substrate reduction activities of the nitrogenase enzyme while other conditions were held constant. This result confirms the critical role of belt-sulfur sites in nitrogenase catalysis.

TABLE OF CONTENTS

LIST OF TABLES

LIST OF FIGURES

LIST OF ABBREVIATIONS

Ar ..... Argon

DMSO ..... Dimethyl Sulfoxide

EQ ..... Equilibrium

Fe-S ..... Iron-sulfur

His ..... Histidine

ICP-OES ..... Inductively coupled plasma optical emission spectroscopy

IMAC ..... immobilized metal affinity chromatography

IPTG ..... Isopropyl β-d-1-thiogalactopyranoside

Kan ..... Kanamycin

Mo ..... Molybdenum

OD ..... optical density

ppb ..... parts per billion

ppm ..... parts per million

PSMF ..... phenylmethylsulfonyl fluoride

rpm ..... revolutions per minute

SAM ..... *S*-adenosyl-L-methionine

Strep ..... Streptomycin

CHAPTER ONE: GLOBAL RELEVANCE

Nitrogen is an essential element for sustaining life on earth as it is the building block for proteins and nucleic acids. Over 78 % of the air on Earth is composed of nitrogen gas (N_2), yet the N≡N triple bond is so strong that it is hard to be broken down and subsequently made available for most organisms (Global Climate Change: Evidence, 2016). Diazotrophs are a class of prokaryotes that have the unique capacity to convert N_2 into ammonia (NH_3) in a process called biological nitrogen fixation. The reduced nitrogen in NH_3 then serves as a usable source of nitrogen by other species. Such nitrogen fixation is made possible with the aid of the metalloenzyme nitrogenase, which accounts for approximately 60% of reduced nitrogen globally (Kim, 1994).

The nitrogenase enzyme of *Azotobacter vinelandii*, a free-living soil bacterium, can reduce a wide variety of substrates. Best-known for its ability to reduce the atmospheric dinitrogen (N_2) to ammonia (NH_3), it can also reduce CO and CO_2 to hydrocarbons. Both reactions are especially relevant for the energy-related area; in particular, ammonia is a clean, carbon-free biofuel other than being an important fertilizer and a versatile precursor to other nitrogen-containing compounds (Jørgensen, 2008). Other than N_2 and CO/CO_2, nitrogenase can also reduce alternative substrates, such as C_2H_2, CN^-, N_3^- and H^+, with the reduction of C_2H_2 to C_2H_4 serving as a routine assay for a quick evaluation of nitrogenase activity (Hu, 2022).

The balanced reaction of N_2 reduction catalyzed by nitrogenase is depicted as follows:

$$N_2 + 8H^+ + 8e^- + 16MgATP \rightarrow 2NH_3 + H_2 + 16MgADP + 16P_i$$

(e^- is electron; P_i is PO_4^{3-})

Through the hydrolysis of 16 equivalents of ATP, substrate reduction takes place with 8 electrons and 8 protons. The strong triple bond in N≡N dinitrogen is broken into single N-H bonds in ammonia. This process occurs naturally under ambient conditions. In contrast, the industrial version of nitrogen fixation via the Haber-Bosch process demands high temperatures (>450 °C), high pressures (>200 atm), as well as an iron-based catalyst. The reaction scheme is as follows:

$$N_2 + 3H_2 \rightarrow 2\ NH_3$$

This process is highly energy-demanding and contributes to up to 3% of global carbon dioxide and nitrous oxide greenhouse gas emissions (González-Cabaleiro, 2021). The Institute for Industrial Productivity stated that in 2010, the Haber-Bosch process generated 451 million CO_2, accounting for 1.2 % of global CO_2 emissions (Boerner, 2019). Thus, it is more than reasonable that the nitrogenase enzyme has been extensively studied during the past decades with the hope to attain knowledge that could inform development of strategies for energy-efficient and environment-friendly production of NH_3 in the future.

CHAPTER TWO: NITROGENASE COMPONENT AND ASSOCIATED METALLOCLUSTERS

Three forms of homologous nitrogenases have been identified to date: the molybdenum-based (Mo), vanadium-based (V) and iron (Fe) only-nitrogenases, which differ in their heterometals (Mo, V and Fe) but all arise from a common ancestor (Hu, 2013). The predominant isozyme Mo nitrogenase from the bacteria *Azotobacter vinelandii*, has been the best-studied and will be the subject of study in this research project.

The Mo nitrogenase is composed of two oxygen-sensitive metalloproteins: (1) the iron protein (Fe protein), or NifH; and (2) the molybdenum-iron protein (MoFe protein), or NifDK (see Figure 1A). NifH is a γ_2-dimeric protein consisting of a MgATP binding site within each subunit, and a [Fe_4S_4] cluster at the subunit interface. NifDK is a $\alpha_2\beta_2$-heterotetrameric protein. It houses two metallocofactors per αβ-dimer: a [Fe_8S_7] P-cluster that bridges between α- and β-subunits (see Figure 1B); and a [$MoFe_7S_9C$-homocitrate] M-cluster (also called FeMoco or cofactor) that resides in the α-subunit (see Figure 1C and Figure 2). The cluster is linked to a protein backbone through the amino acid residues cysteine and histidine. A homocitrate entity is coordinated to Mo through bidentate ligation (Spatzal, 2016). The two components of Mo nitrogenase work together to perform substrate catalysis. NifH is the reductase component that provides electrons for NifDK. Additionally, it aids in NifDK assembly. NifDK is the catalytic component where substrate reduction takes place. NifDK will be the independent variable of this research project.

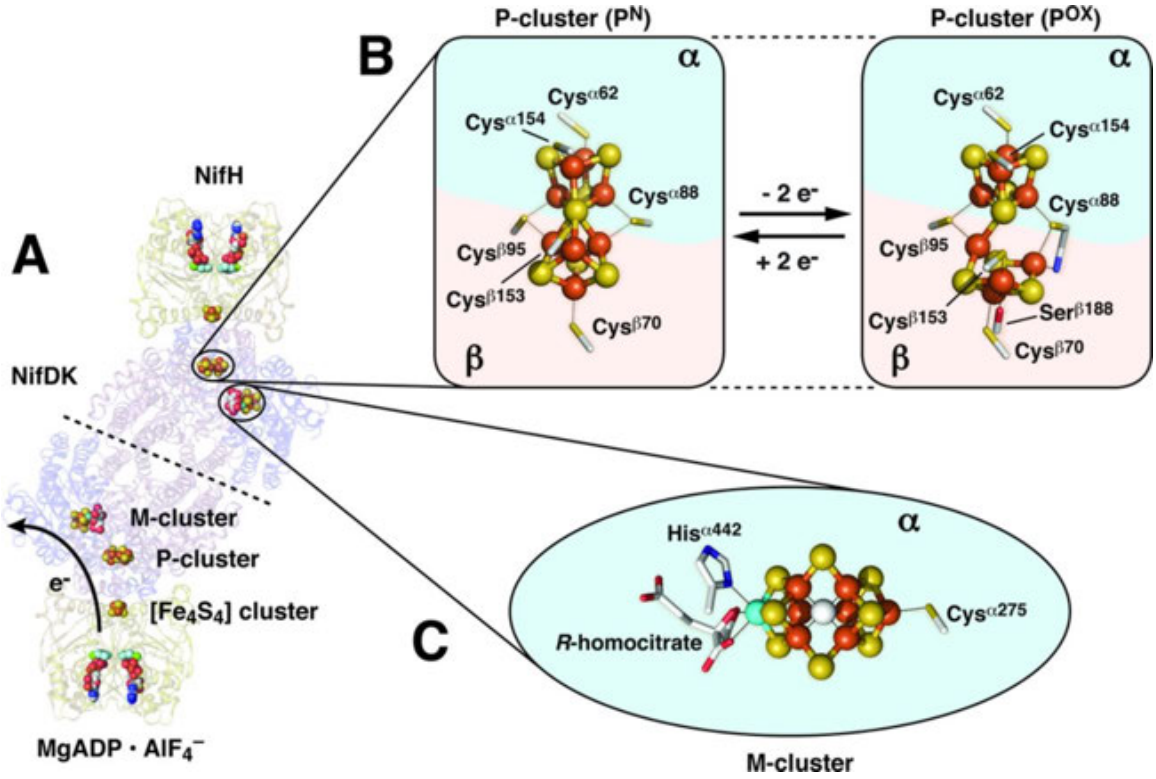

Figure 1: (A) Crystal Structure of ADP•AlF_4^- Stabilized Mo-Nitrogenase. Mo-nitrogenase complex consists of two components: NifH (reductase component) and NifDK (catalytic component). The arrow shows the direction of electron flow during substrate reduction: ATP binds to NifH protein and, upon ATP hydrolysis, electrons flow from the [Fe_4S_4] cluster of NifH to the P-cluster and then to the M-cluster. M-cluster is the site of substrate reduction when sufficient electrons are supplied. **(B) Structure of P-Cluster in NifDK.** P-cluster's main function is to mediate the interprotein transfer of electrons from the [Fe_4S_4] cluster of NifH to the M-cluster of NifDK. Depending on its level of oxidation, P-cluster adopts a variety of conformations. The left panel shows the resting state of the P-cluster, named P^N, where it exists in an all-ferrous form. The right panel shows the two-electron oxidized state of the P-cluster: named P^{OX} or P^{2+}. P-cluster can exist in two other oxidized states, named P^+ and P^{3+}, respectively. **(C) Structure of M-Cluster in NifDK.** M-Cluster is one of the most complex metal cofactors known to date. More details are under Figure 2. Atoms are colored as follows: Fe, orange; S, yellow; Mo, cyan; C, light grey; N, blue; O, red; Mg, green; Al, dark grey; F, light blue (Figure taken from Hu, 2017).

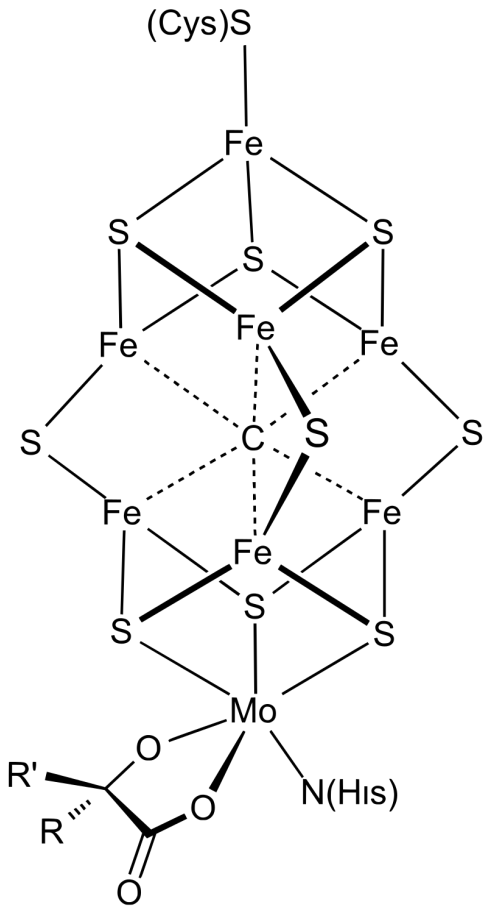

Figure 2: Structure of M-Cluster in NifDK. This [$MoFe_7S_9C$-homocitrate] cluster can be viewed as one Fe_4S_3 cluster and one $MoFe_3S_3$ cluster, connected by 3 sulfide ligands. The environments surrounding these 3 sulfur atoms are the focus of this research project and will be also referred to later as the belt-sulfur sites. A central carbide ion connects with six surrounding iron atoms in a trigonal prismatic arrangement. The molybdenum end and the opposite iron end of the M-cluster are anchored by a histidine and a cysteine ligand, respectively. A homocitrate entity is coordinated to Mo through bidentate ligation and anchored by a lysine residue (Spatzal, 2016).

CHAPTER THREE: SUBSTRATE REDUCTION BY NITROGENASE COMPLEX

During substrate catalysis, the two components of nitrogenase, NifH and NifDK transiently associate with each other to form a functional complex. Specifically, incoming ATP binds to the reduced NifH induces a conformational change in NifH that allows association with NifDK. Subsequently, two ATP molecules are hydrolyzed concomitant with the transfer of one electron to the M-cluster of NifDK (Hu, 2017). Catalysis by nitrogenase relies on the NifH and NifDK to undergo multiple cycles of association and dissociation to transfer electrons from the [Fe_4S_4] cluster of NifH, through the P-cluster, and eventually to the M-cluster, where substrate reduction occurs upon accumulation of a sufficient amount of electrons (see Figure 3).

The mechanism of electron transfer from NifH to NifDK is a highly controlled process. It can only occur with ATP hydrolysis, with the release of the phosphate ion being the rate-limiting step. In addition, crystal structures have shown that the two equivalents of MgATP bound asymmetrically to NifH, signaling sequential rather than concerted hydrolysis (Tezcan, 2015). Cooperative binding of nucleotides to NifH was also observed where the second equivalent of MgATP binds to NifH with up to 15-fold higher affinity after the first equivalent binds (Lanzilotta, 1999). Thus, the sequential ATP hydrolysis and the conformational change that follows the first hydrolysis also contribute to preventing the backflow of electrons.

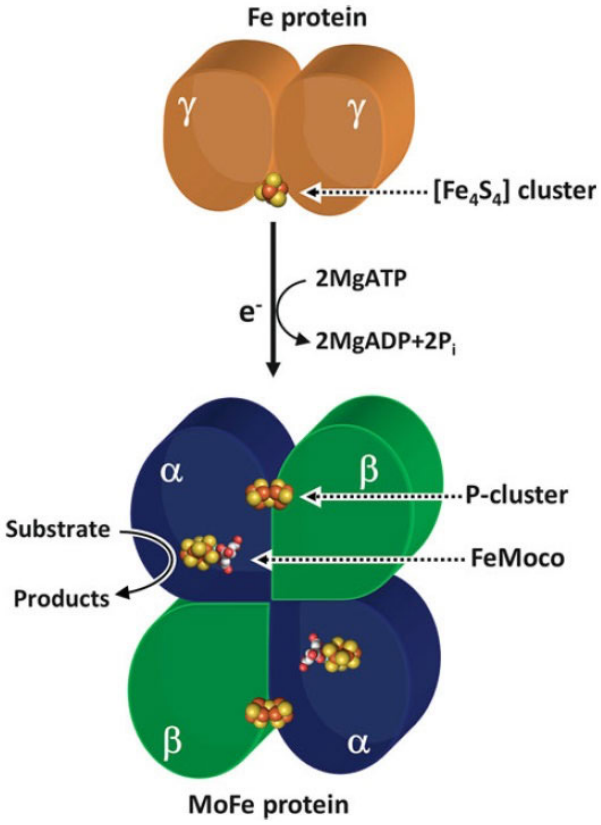

Figure 3: Electron Flow Diagram. Upon ATP hydrolysis, electrons flow from the [Fe_4S_4] cluster of Fe protein (NifH), via the P cluster, to the FeMoco (M-cluster) of NifDK, where substrate reduction occurs (Figure taken from Hu, 2017).

CHAPTER FOUR: BIOSYNTHESIS OF THE P CLUSTER

The biosynthesis of the nitrogenase protein begins with the construction of $[Fe_4S_4]$ clusters, which serve as the building blocks for both P-cluster and M-cluster in NifDK. The synthesis of $[Fe_4S_4]$ clusters requires the action of NifS and NifU, with NifS serving as a pyridoxal phosphate-dependent cysteine desulfurase that donates sulfur to NifU for the sequential formation of $[Fe_2S_2]$ and $[Fe_4S_4]$ clusters (Hu, 2012).

The P-cluster is synthesized *in situ* in a stepwise manner. NifH is critical for P-cluster formation. Characterization of NifDK variant with a deletion mutation of the gene *nifH* showed no formation of P-cluster. Only a precursor form of P-cluster called P*-cluster formed. P*-cluster differs from the $[Fe_8S_7]$ P-cluster in that it is an atypical, $[Fe_4S_4]$-like cluster pair.

The two P-clusters occupying each αβ-subunit pair on NifDK are formed stepwise at different rates (see Figure 4). The formation of the first P-cluster from P*-cluster is rather fast, requiring only NifH. The formation of the P-cluster on the second αβ-subunit requires NifZ, a possible chaperone-like protein to function alongside NifH. A lack of the *nifZ* gene results in one P-cluster in one αβ half and a P*-cluster in the other half. In both cases, NifH acts as an ATP-dependent reductase and reductively couples each $[Fe_4S_4]$-like cluster pair (P*-cluster) into a mature $[Fe_8S_7]$ entity (P-cluster) (Hu, 2013).

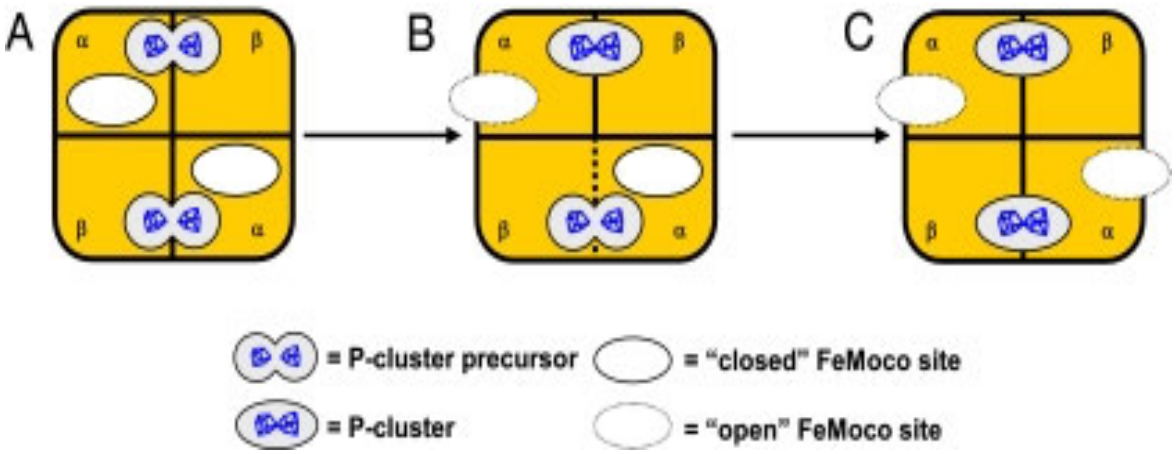

Figure 4: P-cluster Formation Mechanism. The two P-clusters are generated in a stepwise manner, namely, one P-cluster is formed before the other. The successful maturation of P cluster from precursor P*-cluster allows the site for M-cluster to change into an open conformation to allow M-cluster insertion. The necessary components for P-cluster formation are NifH, MgATP, NifZ, and a reductant, dithionite (Figure taken from Lee, 2009).

CHAPTER FIVE: BIOSYNTHESIS OF THE M-CLUSTER

The M-cluster (or cofactor) is synthesized *ex situ* before it is transferred to its final binding site in NifDK. Notably, the insertion of M-cluster into NifDK can only occur once the P-clusters are fully assembled, which renders the cofactor site accessible (Hu, 2013).

The process of M-cluster assembly requires a series of nitrogenase-related proteins (Figure 4). As with the P-cluster (see above), the biosynthesis of the M-cluster begins with synthesis of $[Fe_4S_4]$ clusters by NifS and NifU. A pair of $[Fe_4S_4]$ units (designated the K-cluster) are then transferred to NifB, a radical *S*-adenosyl-L-methionine (SAM) enzyme to assemble a $[Fe_8S_9C]$ precursor of the M-cluster (designated the L-cluster). Characterization of NifDK variant with a deletion of the gene *nifB* has shown a P-cluster containing but M-cluster deficient protein (Δ*nifB* NifDK), proving NifB to be critical for M-cluster formation. The assembly of an L-cluster from a K-cluster involves a series of radical SAM-dependent reactions (see Figure 6). The overall result is the addition of a carbon atom and a sulfur atom concomitant with the coupling and rearrangement of a $[Fe_4S_4]$ cluster pair (K-cluster) into an $[Fe_8S_9C]$ entity (L-cluster).

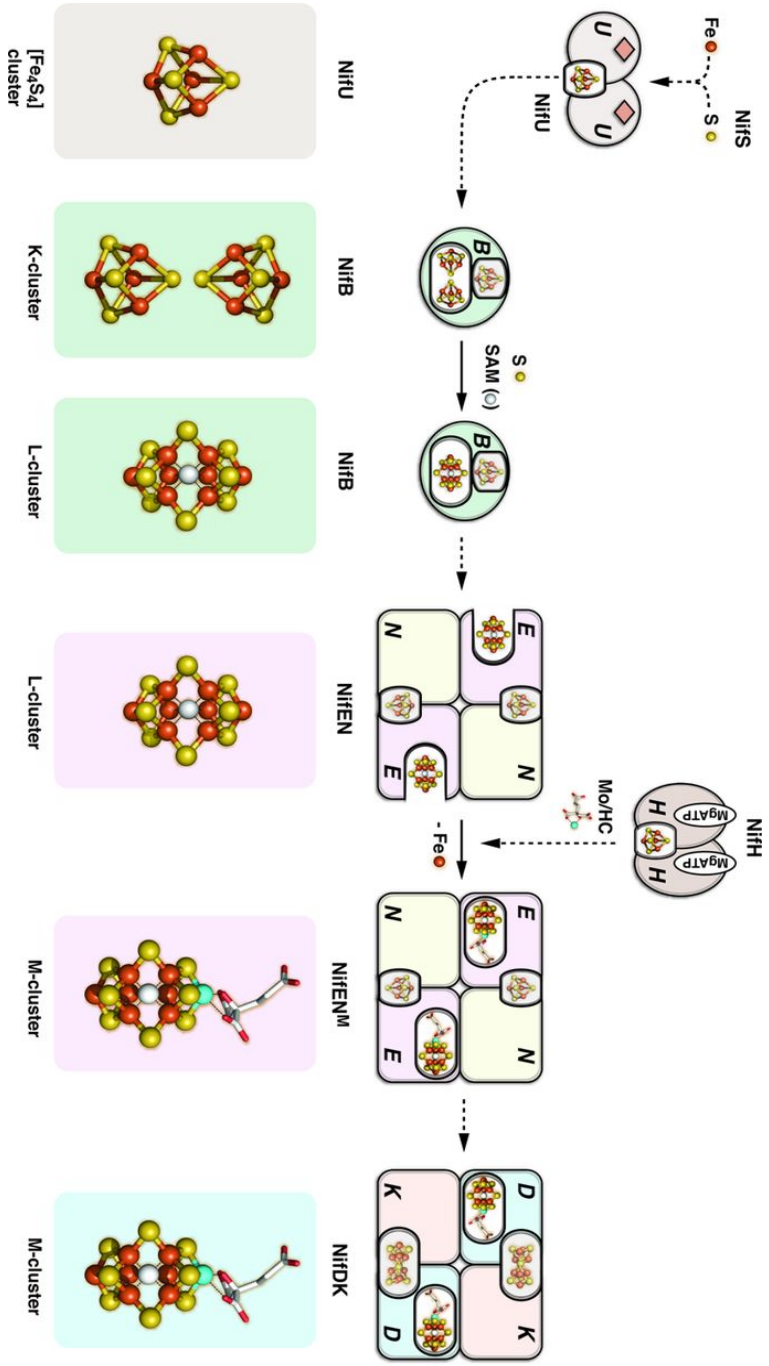

Figure 5: M-Cluster Assembly Pathway. FeS units flow through the following proteins to finally arrive at NifDK as a fully matured M-cluster: NifU-NifS → NifB → NifEN → NifDK. NifU and NifS work together to produce $[Fe_4S_4]$ clusters. A pair of $[Fe_4S_4]$ clusters (K-cluster) is then delivered to NifB, where it is converted to an $[Fe_8S_9C]$ precursor (L-cluster) through a series of radical SAM-dependent reactions. Upon transfer to NifEN, the L-cluster is matured into an M-cluster upon insertion of molybdenum and homocitrate (HC) by NifH. This step leads to a conformational change in NifEN that signals the export and insertion of the M-cluster into its destined location in NifDK, where it carries out substrate reduction. The diamonds on NifU represent $[Fe_2S_2]$ units. Atoms are colored as follows: Fe, orange; S, yellow; Mo, cyan; C, light grey; N, blue; O, red (Figure taken from Sickerman, 2017).

Once generated on NifB, the L-cluster is transferred to NifEN, the next biosynthetic scaffold that converts the L-cluster to a mature M-cluster. Subsequently, NifH interacts with NifEN and delivers molybdate (MoO_4^{2-}) and homocitrate to the Mo-free L-cluster on NifEN, converting the L-cluster to an M-cluster upon incorporation of molybdenum and homocitrate.

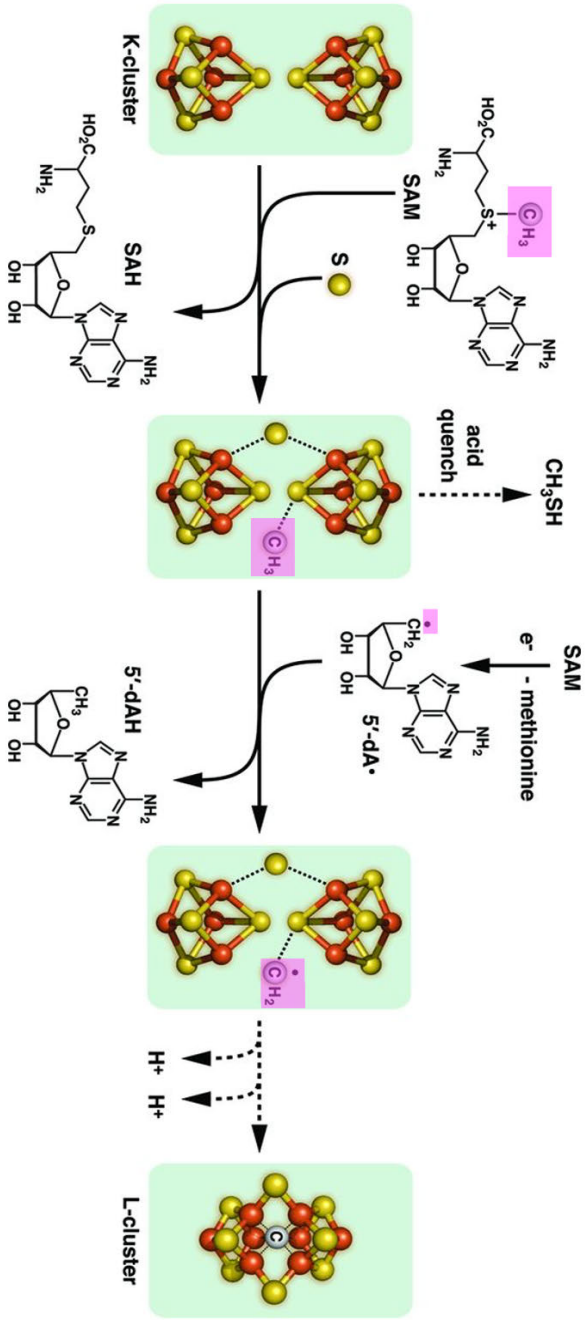

Figure 6: Radical SAM-Dependent Formation of L-Cluster. The general mechanism of SAM reactions involves homolytic cleavage of SAM to yield a 5'dA radical. In this case, two equivalents of SAM are used for the conversion of a K-cluster (a $[Fe_4S_4]$ cluster pair) to an L-cluster (an $[Fe_8S_9C]$ precursor to the M-cluster). The first equivalent of SAM contributes a methyl group to the K-cluster. The second equivalent of SAM undergoes homolytic cleavage at a SAM-responsive $[Fe_4S_4]$ cluster (not shown in the figure) to yield a 5'dA radical, which then abstracts a hydrogen atom from the K-cluster-bound methyl group to generate a methylene radical ($S–CH_2·$). This event initiates the coupling and rearrangement of the two $[Fe_4S_4]$ clusters concomitant with the deprotonation of $S–CH_2·$ into a central carbide. Incorporation of an additional sulfur atom completes the formation of an L-cluster on NifB. Atoms are colored as follows: Fe, orange; S, yellow; C, light grey (Figure taken from Sickerman, 2017).

Upon maturation of the L-cluster into an M-cluster, NifEN likely undergoes structural changes that facilitates the transfer of the M-cluster from NifEN to NifDK. NifEN and NifDK share sequence and structural similarities with each other; in particular, both proteins contain similar cofactor binding sites, though the site in NifEN has lower affinity than that in NifDK that permits the transfer of the M-cluster from the former to the latter site (Sickerman, 2017). Once the negatively charge M-cluster is deposited onto the surface of NifDK, it is inserted along a positively charged cofactor-insertion pathway that consists of three major regions (see Figure 7): (1) a "lid loop" region (including $His^{\alpha 362}$) that could serve as the initial docking point for the M-cluster; (2) a "His triad" (comprising $His^{\alpha 274}$, $His^{\alpha 442}$ and $His^{\alpha 451}$) that could serve as a transient cofactor-binding site midway down the cofactor insertion path; and (3) a "switch/lock" region (consisting of $Trp^{\alpha 444}$ and $His^{\alpha 442}$) that undergoes a switch in position between the $Trp^{\alpha 444}$ and $His^{\alpha 442}$ residues that allows the bulky side chain of $Trp^{\alpha 444}$ to "lock" the M-cluster in its final binding site in the α-subunit of NifDK (Hu, 2007).

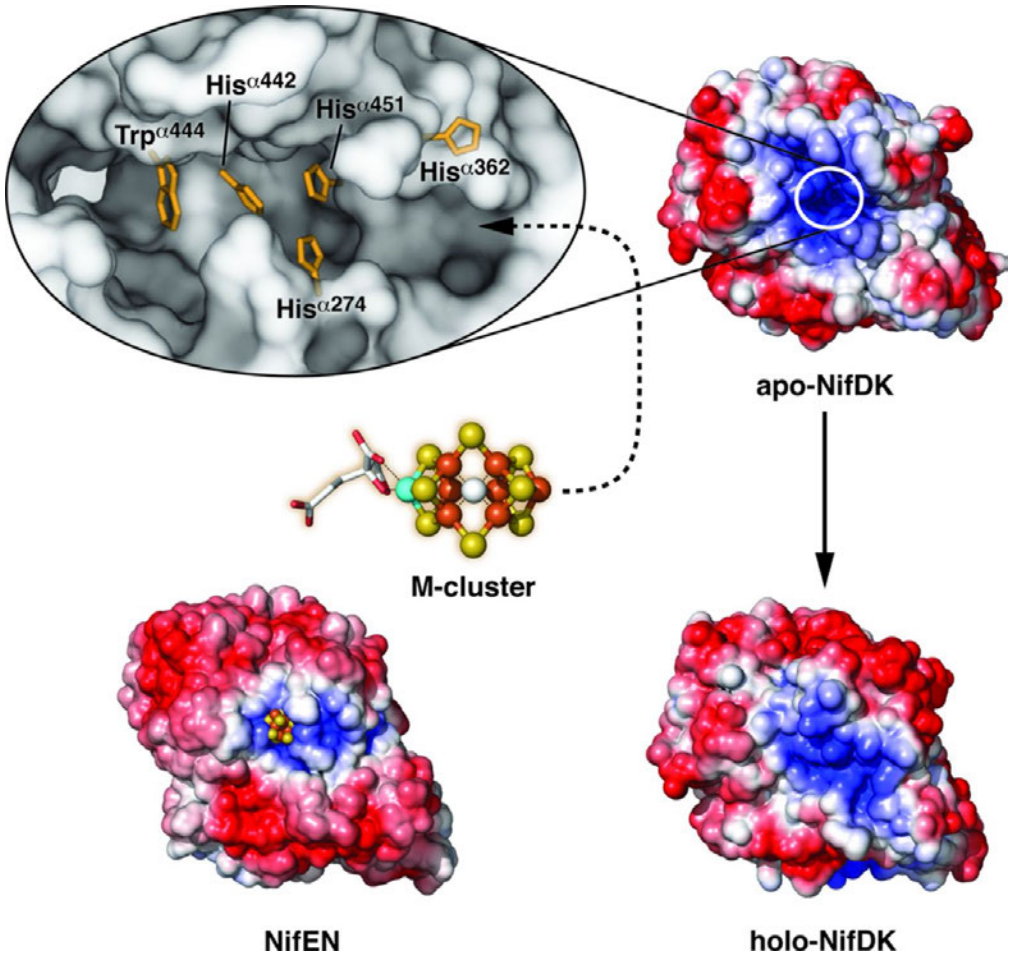

Figure 7: Transfer and Insertion of M-Cluster into Its Final Binding Site. The M-cluster is transferred from the low-affinity binding site in NifEN to the high-affinity binding site in NifDK upon protein-protein interaction. Once it is transferred to the surface of NifDK, the M-cluster first interacts with the "lid loop" (containing His$^{\alpha 362}$), which serves as the initial docking site for the cofactor. Subsequently, the M-cluster interacts with the "His triad" (comprising His$^{\alpha 274}$, His$^{\alpha 442}$ and His$^{\alpha 451}$), which transiently interacts with the cofactor midway down the insertion path. Finally, the M-cluster interacts with the "switch/lock" (consisting of Trp$^{\alpha 444}$ and His$^{\alpha 442}$), which undergoes a swap in position between Trp$^{\alpha 444}$ and His$^{\alpha 442}$ that allows the bulky side chain of Trp$^{\alpha 444}$ to "lock" the M-cluster in its final binding site. top right: apo-NifDK without an M-cluster, showing the accessibility of a positively charged cofactor insertion path. bottom left: cofactor-bound NifEN, showing an "open" cofactor-binding site. bottom right: cofactor-bound holo-NifDK, showing a "closed" cofactor-binding site that buries the cofactor (no longer visible) in the α-subunit of NifDK (Figure taken from Sickerman, 2017).

MATERIALS AND METHODS

Table 1: NifDK Variants with Corresponding Belt-Sulfur Sites. I was responsible for YM534 and YM564 variants. The data of the other variants were collected by my lab mate and served as comparison in the Results and Discussion sections.

NifDK Variants:	Corresponding Belt-Sulfur Sites:
YM531 (H195E)	S2B
YM532 (H195Q)	S2B
YM533 (Q191K)	S2B
YM534 (R96L)	S5A
YM535 (G356/357A)	S3A
YM536 (G356L)	S3A
YM537 (G357L)	S3A
YM564 (R96G/97G)	S5A

Heat-Shock Transformation

A frozen stock of competent cells of a parent strain derived from *E. coli* BL21(DE3) was thawed in an ice bath for 20 minutes. During the thawing period, two plasmids were prepared for transformation: (i) pRSF-*nifHMZ* (Kanamycin resistant) and, (ii) pCDF-*AvnifD*(R96G/R97G)-K (Streptomycin resistant). The *nifDK* genes with mutations of amino acid residues 96 and 97 (Both were mutated from Arginine to Glycine) were synthesized by Genescript (Piscataway, NJ). The overall goal was to test the effect of the double mutation on the catalytic ability of NifDK.

DNA plasmids were spun down at 4000 rpm for 2 minutes. 40 μL of Invitrogen™ TE buffer (Thermo Fisher Scientific) was added to solubilize the DNA for extraction.

The plasmids were vortexed for 10 seconds to well mix DNA with TE buffer. The plasmids were spun down again to allow residual liquids on the sides to collect at the bottom. After competent cells thawed, 1 µL of pRSF-*nifHMZ* plasmid and 1 µL of pCDF-*AvnifD*(R96G/R97G)-K plasmid were pipetted into competent *E. coli* cells. The vial containing competent cells and the two plasmids were incubated on ice for two hours. During this time, a 42 °C water bath was prepared for heat-shock. After incubation, the competent cells with the two plasmids were heat shocked in the hot water bath for 45 seconds. The cells were then put on ice for two minutes for recovery. 0.5 µL of pre-warmed S.O.C. medium containing nutrients for *E. coli* cells was added to the cells as a final step to promote cell recovery and to obtain maximal transformation efficiency. The cells were put in an incubator shaker (New Brunswick Scientific) for one hour for outgrowth. The shaker was set at 37 °C and 200 rpm.

Plating and Incubation

LB agar plates containing streptomycin and kanamycin were prepared for plating. Two concentrations of the transformed cells were plated (see Figure 8): (i) 50 µL of cells were spread on plate #1 using a sterile spatula; (ii) The rest of the cells were spun down in a centrifuge at 200 rpm for 3 minutes. The resulting vial contained cell concentrate at the bottom as pellet. Supernatant above the pellet was disposed, thereby achieving higher concentration. When enough supernatant was taken out until the liquid level matched the pellet height, the cells were resuspended in the remaining supernatant via gentle stirring with a pipette tip. Next, the concentrated cells were spread on plate #2. Both plates were

incubated in a Heratherm incubator (Thermo Scientific) upside down at 37 °C for 15 hours. During this time, cell colonies formed.

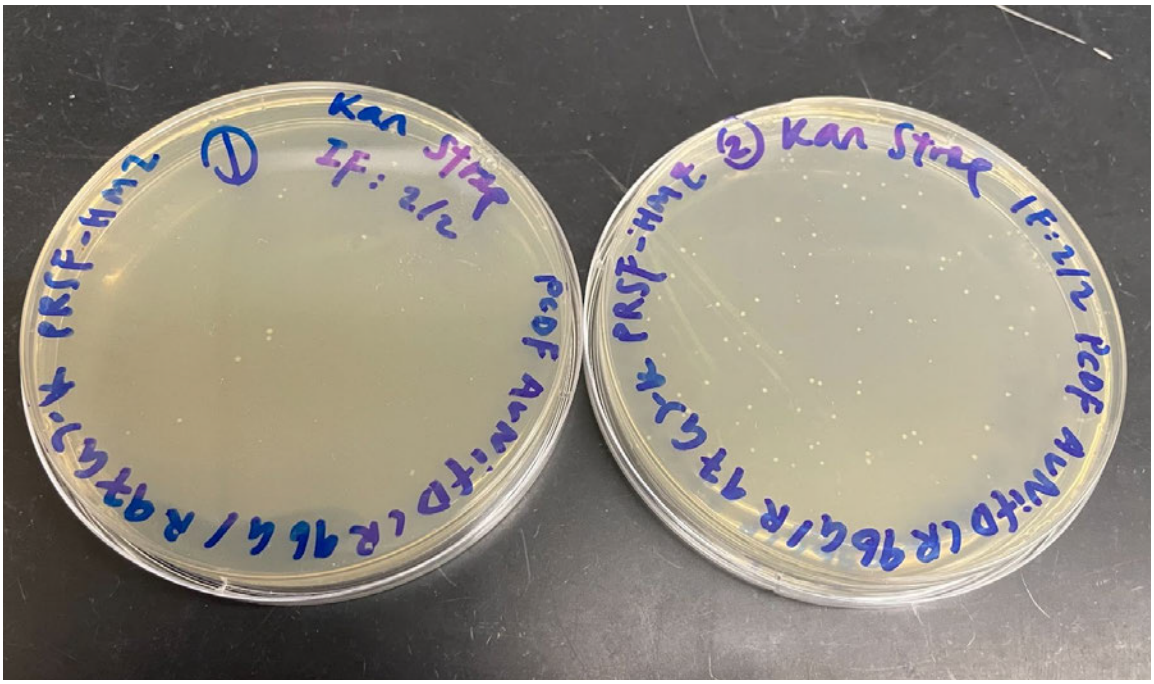

Figure 8: Cell Colonies of Transformed *E. coli*. After incubation, plate #1 (left) had significantly lower numbers of colonies compared to plate #2, which was reasonable since plate #1 contained less concentrated *E. coli* cells. Plate #1 had about 12 colonies and plate #2 (right) had about 76 colonies.

Freezer Stock Preparation

Day 1:

200 mL LB media was prepared for bacterial culture growth. 160 µL kanamycin (Kan) and 160 µL streptomycin (Strep) were added. 17 cell colonies were selected: 5 colonies from plate #1 and 12 colonies from plate #2 (see above). 4 mL of the prepared LB media was added to 17 sterile culture tubes. For every culture tube, one colony was picked using a sterile pipette tip and ejected into the tube. The culture tubes were put in

an incubator shaker (New Brunswick Scientific) for overnight growth at 37 °C and 200 rpm.

Day 2:

Five of the culture tubes showed cell growth and were used to prepare freezer stocks. Dimethyl Sulfoxide (DMSO) was used as cryoprotectant agents to generate these stocks. DMSO decreases the melting point of the medium, preventing ice crystal formation during freezing and storage at -80 °C, which can harm cells and result in cell death (Chen, 2013). 1 mL of DMSO was pipetted into each culture tube. 2 mL of the final solution of each tube was transferred into a 2 mL pyro vial. The five pyro vials were labeled K1 through K5 and stored at -80 °C as freezer stocks for future use.

Preculture Preparation for Fermenter Growth

Of the five freezer stocks (K1-K5), K2 was used to prepare a preculture. 160 µL of Kan and 160 µL of Strep were added to a 200 mL LB media to allow only Kan- and Strep- resistant *E. coli* cell growth. A pipette tip was used to scoop up approximately 200 µL of K2 freezer stock. The pipette tip with K2 *E. coli* cells was then ejected into the LB media flask. The cell media was put on an incubator shaker at 37 °C and 200 rpm for overnight growth. Cell growth was observed after overnight growth.

Sterilization of Fermenter

E. coli cells expressing nitrogenase NifDK variants were grown in 10 L fermenters for protein expression.

Two 10 L fermenters were sterilized. A media of 200 g NaCl, 100 g yeast, 200 g peptone, 209 g 3-(*N*-morpholino)propanesulfonic acid, 23 g NaOH, 90 g glucose, and 4 L of H_2O was prepared. Each fermenter was filled in the order of 2 L H_2O, 2 L media, 2 L of H_2O. The fermenter temperature was set to 37 °C and AUTO. Airflow and agitation were set to AUTO. Sterilization was then initiated and lasted for approximately two hours.

Fermentation and Protein Expression

After sterilization, 5 g ammonium iron citrate, 0.2 g Kan, and 0.3 g Strep were added to each fermenter. 100 mL preculture (see above) was added to each fermenter. The growth of *E. coli* cells took place at 37°C for approximately two hours.

A turbidity measurement at 595 nm was used to monitor cell growth. H_2O was used as a standard and its optical density (OD) was set to 0 in a Thermo Fisher UV/vis spectrophotometer.

Once the cells reached an OD of around 0.5, the temperature was decreased to 24°C. Also, airflow was turned off and replaced by dinitrogen flow to create an anaerobic environment. 48 g of Isopropyl β-d-1-thiogalactopyranoside **(**IPTG), 42 g of fumarate, and 2.2 g of cysteine were added to each fermenter. IPTG is a molecular mimic of allolactose and induces transcription. *E. coli* cells were allowed to express nitrogenase proteins for approximately 16-18 hours before harvesting.

Cell Harvest

E. coli cells were harvested by centrifugation at 10,000 rpm for 2.5 minutes at 4 °C in a ThermoFisher Scientific Legend XTR centrifuge. The supernatant was disregarded into a waste bucket with a small amount of bleach. The cell paste was collected into a plastic bag and weighed.

Two batches of cells were generated for each *E. coli* strain. The first batch of cell paste of YM564 weighed 32.24 g. The second batch of cell paste of YM564 weighed 20.32 g. (total: 52.56 g)

The first batch of cell paste of YM534 weighed 58.01g. The second batch of cell paste of YM537 weighed 49.84 g. (total: 107.85 g)

The cell pastes were stored with dry ice at -80 °C.

Purification of His-Tagged Nitrogenase Proteins

Due to the air-sensitive nature of the Fe/S clusters of NifDK, its protein purification requires careful handling. An anaerobic environment needs to be maintained throughout the entire process. Therefore, protein purification was carried out in the presence of 100% Argon (Ar) gas.

An equilibration (EQ) buffer was made with 58.4 g NaCl, 100 mL 1 M Tri-HCl at pH 8.0, 200 mL 10% glycerol and 1700 mL H_2O, totaling a volume of 2000 mL. EQ was distributed into four flasks to make 4 solutions: CELL (volume was three times the crude

extract weight: (58.01 + 49.84) *3= 323.55 g. 350 mL was used for proportion reason.), RINSE (250 mL of EQ), WASH (500 mL of EQ), and KO (knockout) (250 mL of EQ). Frozen cell paste was resuspended in CELL and one spatula of deoxyribonuclease and phenylmethanesulfonyl fluoride (PMSF) were added. PMSF functions as a protease inhibitor that prevents the degradation of proteins. Then, EQ, RINSE, and CELL buffers were degassed under vacuum for one hour to create an anaerobic environment. After degassing, sodium dithionite ($Na_2S_2O_4$), a reducing agent to remove O_2, was added in proportion to EQ volume to each flask: 0.087 g to RINSE; 0.1218 g to CELL; and 0.2262 g to EQ.

E. coli cells were lysed under 100% Ar by a Gaulin microfluidizer at 12,000 lb./in^2 for subsequent purification of NifDK proteins. Cells were degassed after lyses for 1 hour to maintain anaerobic conditions to prevent NifDK damage.

RINSE was first poured into the microfluidizer to wash the machine with media. Then, CELL was poured through twice to lyse the cells twice.

At the same time, WASH and KO were degassed with imidazole added. Imidazole is a competitive agent that binds stronger to a immobilized metal affinity chromatography (IMAC) column than Histidine-tagged protein to allow its purification. WASH and KO were used to elute Histidine-tagged NifDK proteins from the column in the next step. 1.362 g of imidazole was added to WASH to create a 40 mM concentration. 4.255 g of imidazole was added to KO to create a more concentrated (250 mM) solution.

Since the nitrogenase proteins are sensitive to O_2, transfer of cell lysates to different containers needs to be done in an Argon glove box. After transfer of cell lysates

into two centrifuge bottles in the glove box, the bottles were centrifuged in a ThermoFisher Scientific Legend XTR centrifuge at 10,000 × *g* for one hour at 4 °C. After centrifugation, the NifDK-containing supernatant was anaerobically collected in a flask in the glove box.

IMAC was performed to purify histidine-tagged NifDK proteins. The histidine-tags of these proteins bind to the Nickel-containing resin of the IMAC column. EQ was first run through the column for half an hour, followed by the cell lysate. A dark band appeared on the blue resin (see Figure 19A) that indicates the attachment of His-tagged NifDK proteins to the column (see Figure 9B). After washing the IMAC column with WASH, His-tagged NifDK protein was eluted from the column using KO that contains a high concentration of imidazole. The appearance of the brown color protein (see Figure 10A) in the tube signals the time to collect the pure proteins into an anaerobic Schlenk flask. Protein collection ended when the color in the tube changed to clear. The elution volume of NifDK of YM564 was 10 mL (see Figure 10B). The elution volume of NifDK of YM534 was 15 mL.

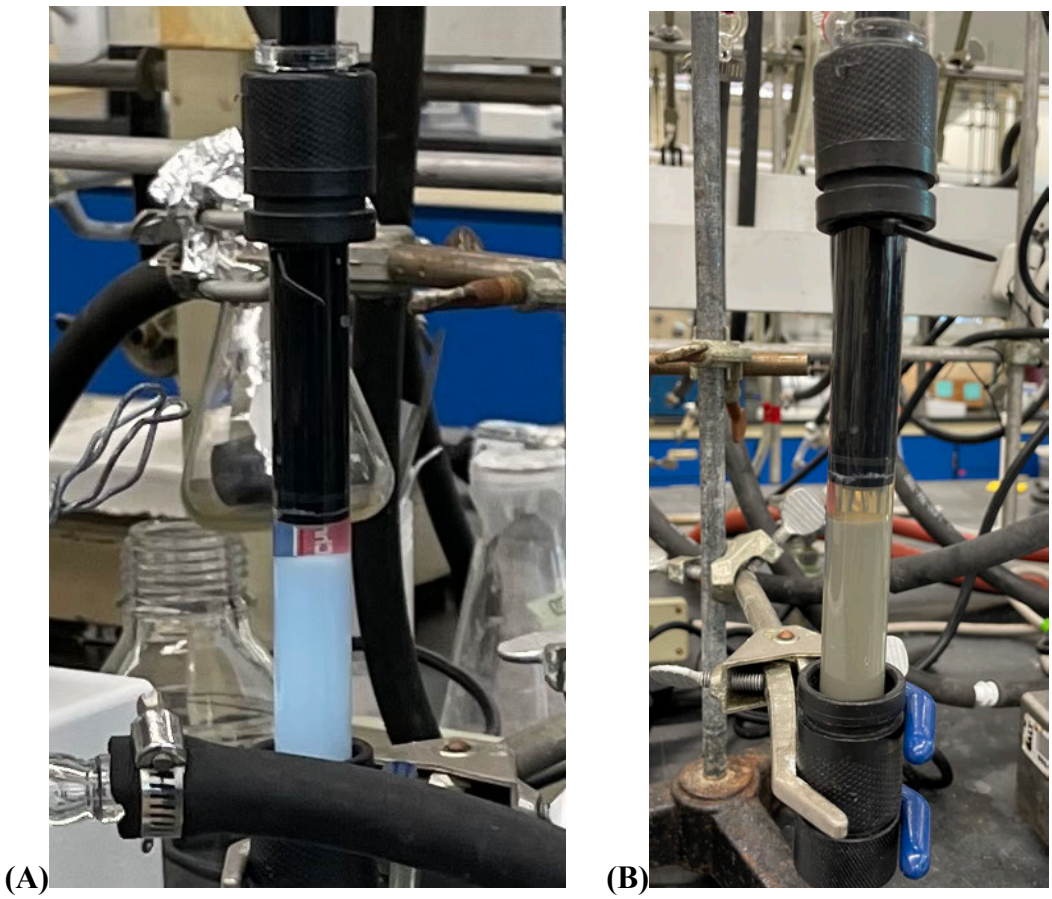

Figure 9: (A) Ni-loaded IMAC Column. (B) His-tagged NifDK bound on the Column. The turning from blue to brown color on the column indicated that NifDK was loaded onto the column.

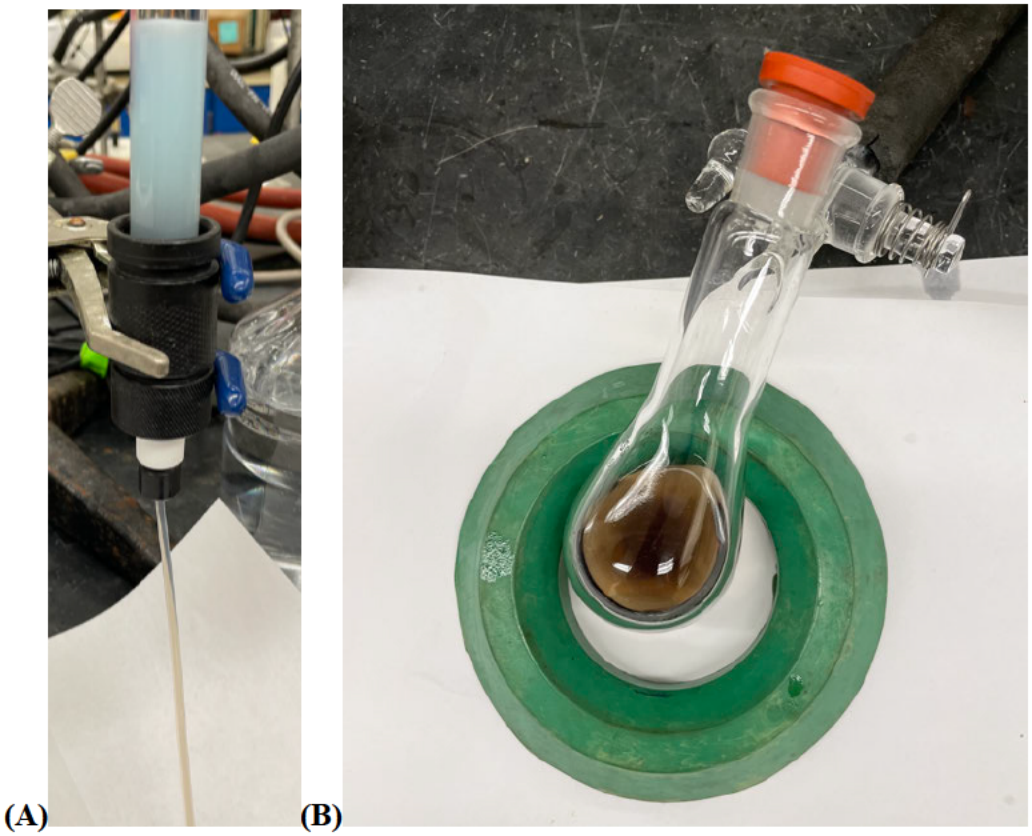

Figure 10: (A) Brown Eluent. The brown colored eluent in the tube contains His-tagged NifDK protein. **(B) Collection of NifDK of YM 564.**

As a final step, the nitrogenase proteins were slowly pipetted into a bowl of liquid nitrogen using an anaerobic, buffer-washed syringe. The proteins became frozen pellets and were collected in a vial. The vial was stored in a liquid nitrogen container for future analysis.

ASSAYS

Bradford Assay

Bradford assay was performed to determine protein concentrations. 10 µL protein (NifDK of YM564, NifDK of YM534, and protein standard) was diluted with 990 µL Milli-Q water. The diluted solution was vortexed to mix. Six standards were distributed to cuvettes according to Table 2. Five samples of NifDK proteins were prepared according to Table 3. 10 mL of Bio-Rad protein assay dye concentrate was diluted with 40 mL Milli-Q water. 2.5 mL of dilute dye was added to each cuvette and incubated for 10 minutes.

Table 2: Six Different Concentrations of the Protein Standard.

Standard	H2O (µL)	0	20	40	60	80	100
	standards (µL)	100	80	60	40	20	0
	Dye (mL)	2.5	2.5	2.5	2.5	2.5	2.5

Table 3: Five Different Concentrations of NifDK Protein.

Protein Sample	H2O (µL)	0	20	40	60	80
	Diluted protein (µL)	100	80	60	40	20
	Dye (mL)	2.5	2.5	2.5	2.5	2.5

The cuvette with 100 µL H_2O was set to 0 % absorbance at 595 nm. Absorbances for the protein standards and NifDK proteins were measured at 595 nm using a UV spectrometer. Protein concentration of NifDK of YM564 was calculated to be 13.09 mg/mL. NifDK of YM534 had a concentration of 8.26 mg/mL.

Gel Electrophoresis

A solution of 5 µL purified protein, 25 µL H_2O, and 40 µL 2 x sodium dodecyl sulfate was prepared for gel electrophoresis. The protein solution was incubated at 95-100 °C for 10 minutes, followed by centrifugation at 21 °C. 1 µL protein solution was loaded onto a 4–15% precast polyacrylamide gel, along with the Precision Plus Protein Kaleidoscope Standards. The gel is shown in Figure 11 of the Results section.

Substrate Reduction Assays

C_2H_2-reduction assays were carried out in 9.5 mL sealed vials, containing 10 % C_2H_2 and 90 % Ar. Each assay contained 25 mM Tris–HCl (pH 8.0), 2.5 mM ATP, 5.0 mM $MgC1_2$, 30 mM creatine phosphate, 0.125 mg of creatine phosphokinase, and 20 mM $Na_2S_2O_4$ (1 mL total volume). The reaction was initiated by adding NifDK proteins, followed by incubation at 30 °C for 10 minutes, quenching with EDTA, and analyzed product formation. To detect C_2H_4 as a product of C_2H_2-reduction, 250 μL of the headspace was injected into a gas chromatography-flame ionization detection (SRI Instruments, Torrance CA) equipped with a packed Poropak N column (Restek, Bellefonte, PA).

The C_2H_4 peak area values were collected in Table 4 and in Figure 12 of the Results section.

Iron Analysis by ICP-OES

17 culture tubes were prepared, 2 tubes for each NifDK variant and 1 empty tube as the blank.

200 µL of concentrated sulfuric acid (H_2SO_4) and 200 µL of concentrated nitric acid (HNO_3) were added to each protein sample (0.5 and 1 ppm for each NifDK variant). The sample mixtures were digested in a heat block at 250 °C for two hours. The addition of HNO_3 and H_2SO_4 were repeated until the culture tubes became colorless, indicating the complete oxidation of all Fe atoms to Fe^{3+} and full digestion of the protein sample. Subsequently, samples were cooled down to room temperature and diluted to a final volume of 7.5 mL with 2.2 % HNO_3. Iron analysis was then performed using inductively coupled plasma optical emission spectroscopy (ICP-OES) using a Thermo Scientific iCAP7000.

Calibration standards were prepared at Fe concentrations of 1 ppb (parts per billion), 5 ppm (parts per million), 7.5 ppm, and 10 ppm. The results of the Fe analysis are shown in Table 5 & Figure 13 of the Results section.

RESULTS

E. coli Yield Versus. Protein Yield

While the *E. coli* cell yield of YM564 (52.56 g) was significantly lower than that of YM534 (107.85 g), the yield of the purified NifDK protein of YM564 (131 mg) was higher than that of NifDK protein of YM534 (66 mg).

This could be due to a variety of reasons. One possibility is that the NifDK protein of YM564 folds better and is more stable compared to the protein purified from YM534. However, more work will be required to determine the reason(s) for the observed difference.

Gel Electrophoresis of Purified NifDK Proteins

Gel electrophoresis was performed to confirm the successful purification of the NifDK proteins.

Precision Plus Protein Kaleidoscope Standards ranging from 10-250 kDa were used to identify the α- and β-subunit (NifD and NifK, respectively) of the purified NifDK proteins based on their known molecular weights (NifD: 55.3 kDa; NifK: 52.1 kDa).

Both subunits were clearly present in case of all eight NifDK variants as shown by the middle two dark blue bands of Figure 11.

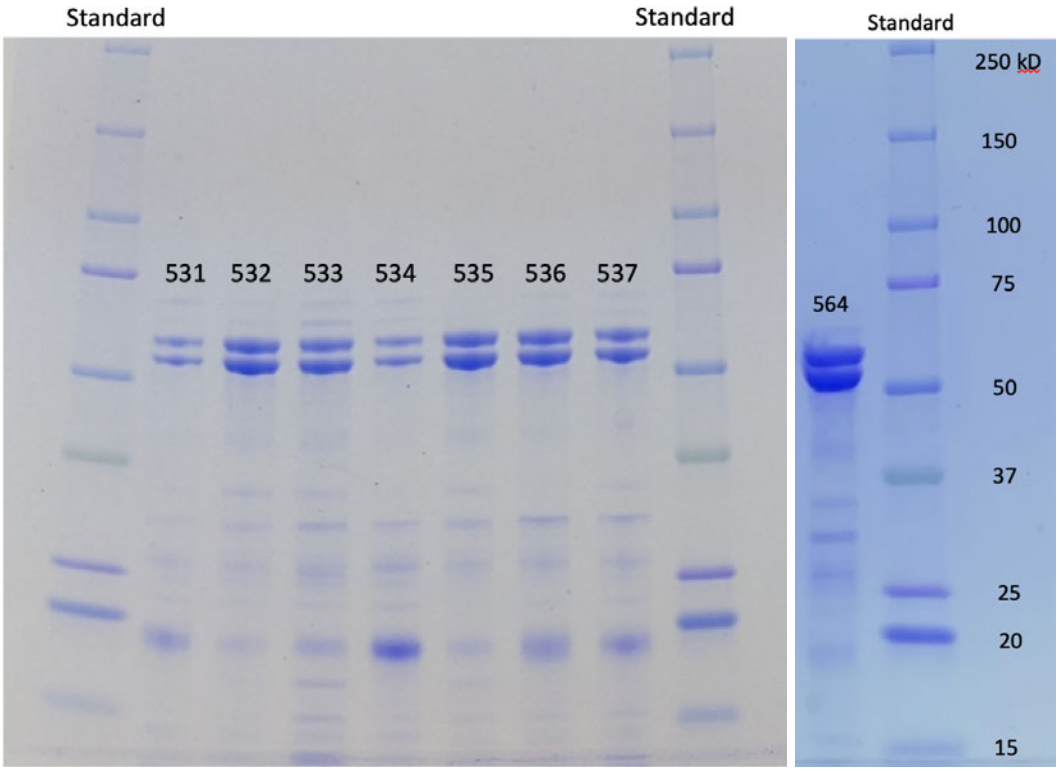

Figure 11: Gel Electrophoresis of NifDK Variants of this Study.

FID Gas Chromatography: Acetylene Reduction Activity

FID gas chromatography was performed to evaluate the level of C_2H_2-reduction that took place in the eight NifDK variants. Results were compared with negative and positive controls to deem significance (i.e. A two-fold increase or decrease would be considered as significant results). The C_2H_4 peak areas were shown in Table 4.

Table 4: C_2H_2 Reduction Activity of the NifDK Variants of this Study. Shown are the numbers of the formed C_2H_4 in the assays. Numbers in red are significantly higher than the negative control. The YM533 NifDK variant is starred because it showed further reduction of C_2H_2 to C_2H_6, an effect that was not observed for any of the other variants.

	C2H4			
	1st	2nd	Mean	Std
YM531	5.41	4.95	5.18	0.33
YM532	11.19	16.24	13.72	3.57
YM533**	10.46	10.95	10.71	0.35
YM534	5.24	5	5.12	0.17
YM535	4.3	4.57	4.44	0.19
YM536	4.56	4.54	4.55	0.01
YM537	4.04	4.55	4.30	0.36
YM564	4.6	4.41	4.51	0.13
neg control 1	5.79	4.96	5.38	0.59
pos control 1	334.55	306.29	320.42	19.98
neg control 2	4.2197	4.66	4.44	0.31
pos control 2	329.22	300.32	314.77	20.44

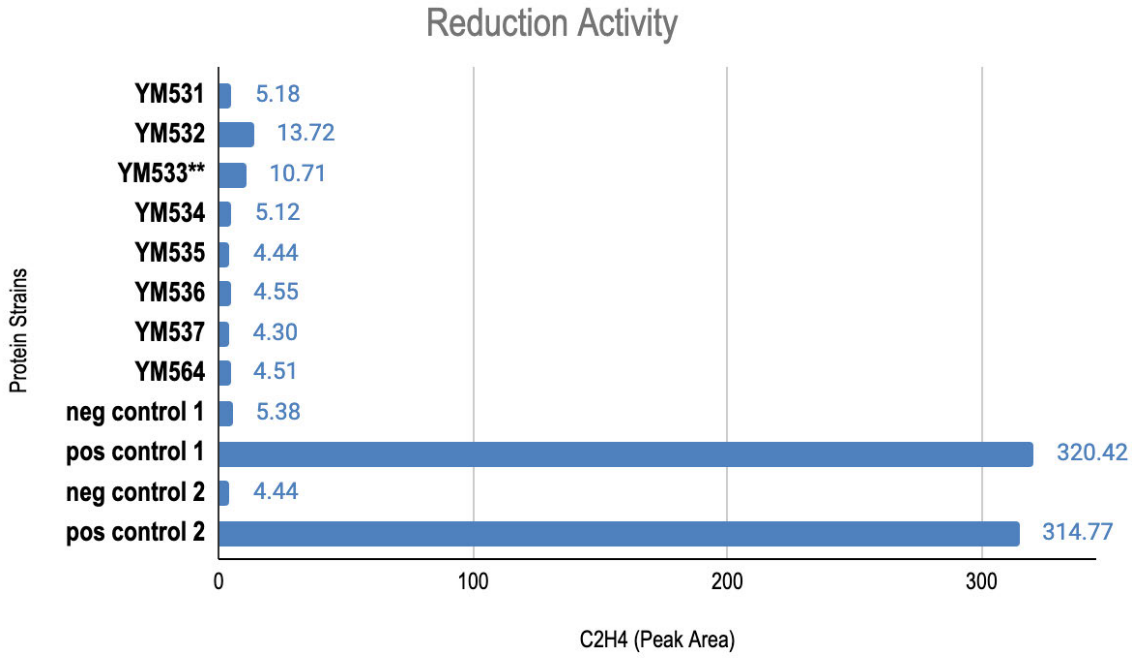

Figure 12: Bar Graph of the Mean Data shown in Table 4.

The positive control represented M-cluster reconstituted wild-type NifDK that shows maximum activity. The negative control represented M-cluster deficient NifDK that does not show activity. The eight NifDK variants were all reconstituted with M-cluster. All NifDK variants contained mutations at the belt-sulfur region of the M-cluster of NifDK to test the ability of these belt-sulfur variants to function in nitrogenase reactivity.

The negative control showed values of C_2H_4 formation of 5.38 and 4.44 (Table 3). Values of 5 in case of the NifDK variants can be considered as being inactive. This was the case for NifDK variants of YM531, YM534, YM535, YM536, YM537, and YM564.

In contrast, NifDK of YM532 and YM533 showed C_2H_4 formation values of 13.72 and 10.71, respectively, which represents a two-fold increase compared to the negative control. This indicated that a low level of C_2H_2-reduction has happened. Nonetheless, the values of C_2H_4 formation were well below the positive controls (Control 1: 320.42; Control 2: 314.77). This indicates that C_2H_4 formation carried out by the two NifDK variants was very inefficient (see Figure 12)

It was interesting to see that NifDK of YM533 showed an additional ethane (C_2H_6) peak in the assays, indicating further reduction of C_2H_4 to C_2H_6. The peak area for NifDK of YM533's first sample was 0.845 (7.87 ppm C_2H_6). The peak area for NifDK of YM533's second sample was 0.9 (8.33 ppm C_2H_6). The mean C_2H_6 value was 8.1 ppm.

Analysis of Iron Contents by ICP-OES

As shown in Table 5 and Figure 13, the iron contents of all eight NifDK variants were lower than the positive control, wild-type NifDK (wild-type MoFe protein). The same amount of ammonium iron citrate was supplied to all *E.coli* strains expressing NifDK variants and wild-type NifDK during cell growth. All NifDK proteins should contain 16 iron atoms if their Fe-containing metal clusters would be fully incorporated during protein assembly in the cell. However, the metabolic pathways of *E. coli* are inherently different compared to that of *Azotobacter vinelandii*. *A. vinelandii* is an obligate aerobic soil bacterium, whereas *E. coli* is facultative anaerobic bacterium that lives in the intestine of warm-blooded organisms (Bothe, 2007).

Introduction of "foreign" nitrogenase genes into *E. coli,* which does not house the nitrogenase enzyme naturally, could lead to a certain level of incompatibility and the observed inefficient biosynthesis. The speed that *E. coli*'s enzymes such as DNA polymerase and RNA polymerase that are used to replicate and express *nifDK* genes could differ from the usual speed *A. vinelandii* takes. This could cause cofactors and protein backbones to form at times that do not cooperate to form functional NifDK. For instance, if the assembly time of the iron-containing M-clusters does not match the assembly time of apo-NifDK in *E. coli*, incorporation of M-clusters into NifDK may be more difficult, as shown by the lower than usual iron contents in all eight NifDK variants.

Table 5: ICP Iron Contents of the Eight NifDK Variants of this Study.

Iron Contents				
	1ppm	0.5ppm	Mean	Std
YM531	10.096	14.048	12.07	2.79
YM532	9.376	10.24	9.81	0.61
YM533	8.288	10.016	9.15	1.22
YM534	6.16	7.072	6.62	0.64
YM535	8.544	12.8	10.67	3.01
YM536	10.768	11.712	11.24	0.67
YM537	5.216	5.376	5.30	0.11
YM564	2.384	3.424	2.90	0.74
wildtype MoFe	16	16	16.00	0.00
		Ave of variants: 8.68		

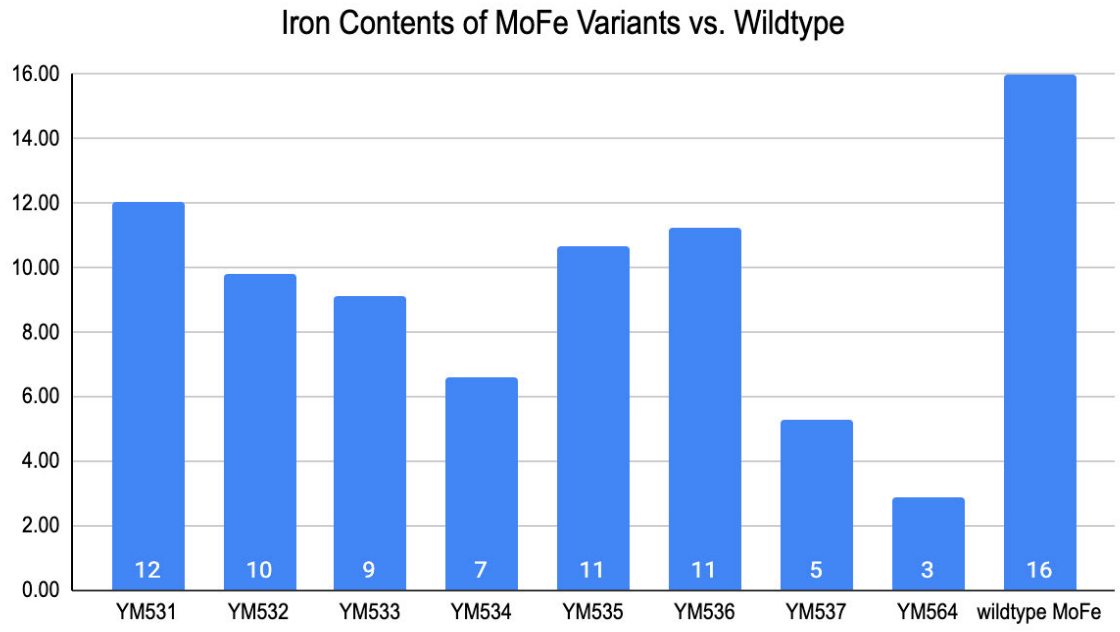

Figure 13: Bar Graph of the Mean Data shown in Table 5.

DISCUSSION

As mentioned in the Abstract section, the belt-sulfur mobilization mechanism proposes an asymmetric displacement of belt-sulfurs of the M-cluster by three dinitrogen species that possibly represent different reduction states of N_2 (see Figure 14).

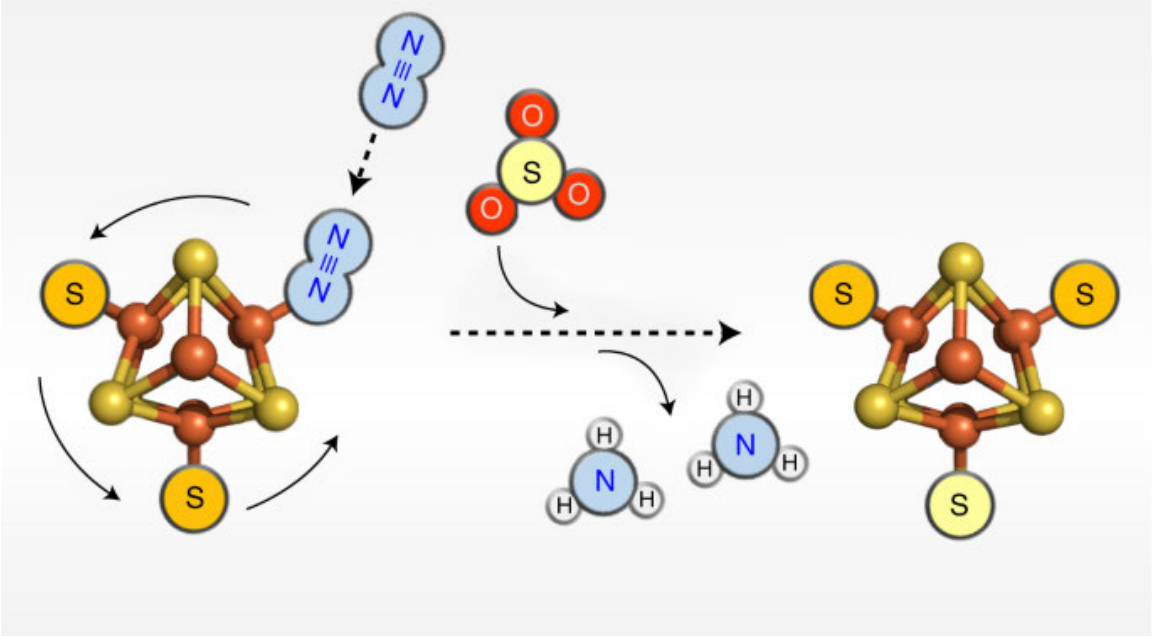

Figure 14: Belt-Sulfur Mobilization Mechanism. Stepwise displacements of three sulfur atoms by **different reduction states of N_2** leads to the release of the product ammonia (NH_3). (Figure taken from Hu, 2022)

Strikingly, each of the three belt-sulfur sites (designated S3A, S5A, and S2B) of the M-cluster of NifDK have distinct amino acids and hydrogen bonding distances that might stabilize substrate binding and/or donate protons that are needed for its reduction. Substrates are proposed to form hydrogen bonds at the S3A site with the amide groups of the protein backbone (α-G356 and α-G537) upon binding to the M-cluster of NifDK. Further reduced substrate intermediates can form hydrogen bonds at the S5A site with the side chain of α-R96 of the protein backbone. This allows H^+ to be transferred to the

reduction intermediate, which leads to the further reduction of this intermediate followed by product release. In addition, it was observed in a previous study that the binding of reduced substrate intermediates to the S2B site caused elongation of the Mo-O7 (hydroxyl) distance of the M-cluster and switched the Mo-homocitrate ligation of the cluster from bidentate to monodentate (Hu, 2022). Together, these results and the resulting mechanistic proposal highlight the crucial involvement of all three M-cluster belt-sulfur sites in substrate binding and reduction.

NifDK of YM534(R96L) and YM564(R96G/R97G) had point mutations in the protein backbone surrounding the S5A site. Acetylene reduction assay showed no activity for both mutants. These results indicate that the amino acid residues 96 and 97 both contribute to an ideal protein environment of the S5A site that is required for acetylene reduction. This observation further suggests that reduced substrate intermediate can no longer form hydrogen bonds with the side chain of R96, which made further reduction impossible. No reduction activity is in line with the proposal that the S5A site is a necessary exit point for reduced products. It is possible that the mutation at the S5A site prevents products from being released. Therefore, no activity was detected by gas chromatographic assays. To compare the iron contents of the two NifDK variants, NifDK of YM564 contained 3 iron atoms per protein compared to 7 iron atoms per protein in case of NifDK of YM534. The lower iron contents of NifDK of YM564 could be due to a more unstable nature of this NifDK variant that contains a double mutation (R96G/R97G) close to its active site.

NifDK of YM531(H195E), YM532(H195Q), and YM533(Q191K) had point mutations in the protein backbone surrounding the belt-sulfur site S2B. While no acetylene reduction was detected for NifDK of YM531, some reduction was observed for NifDKs of YM532 and YM533. Compared to the positive wild-type NifDK control, NifDK of YM533 showed significantly lower reduction activity. Thus, the residue Q191 contributes to the protein environment of the S2B site to a level that impacts the substrate reduction ability. It was also notable that further reduction to ethane was observed in YM533, which did not occur in any other NifDK variants.

NifDKs of YM531(H195E) and YM532(H195Q) had different mutations at the same residue. Interestingly, the two variants showed distinct C_2H_2-reduction activities. NifDK of YM531 showed no C_2H_2-reduction activity while NifDK of YM532 showed low activity. NifDK of YM531 contains a mutation at the active site that changes a positively charged histidine to a negatively charged glutamic acid. This change could create a protein environment where substrate-reduction is no longer supported. In contrast, although the NifDK variant of YM532 also contained a mutation of residue 195, the charge change was less severe from positive to neutral. Therefore, the protein environment might still be able to support a low level of acetylene reduction activity. Overall, NifDK of YM532 showed significantly lower C_2H_2-reduction activity compared to the positive control. This indicates a crucial role of the S2B site of M-cluster for substrate reduction.

NifDKs of YM535(G356A/G357A), YM536(G356L), and YM537(G357L) had point mutations in the protein backbone surrounding the S3Asite, the proposed substrate

entry site. Results from the acetylene reduction assays showed no activity for all three mutants. These results indicate that substrates are potentially not able to interact with M-cluster due to the mutated S3A protein environment. Residues 356 and 357 both contribute the ideal protein environment for substrate binding. Interestingly, a single mutation in either location already leads to the absence of any C_2H_2-reduction activity as shown in NifDK mutants of YM536 and YM537. This is consistent with the proposal that the S3A site of NifDK is critical for substrate reduction and product formation.

Low iron contents in all eight variants indicate that future optimization could be done to achieve better nitrogenase assembly. Increasing the amount of ammonium iron citrate and sulfur atoms supplied during induction could potentially increase the amount of iron cluster formation.

Future work will be required to further elucidate the substrate reduction mechanism of nitrogenase such as trapping intermediates of substrate-reduction at the belt-sulfur sites of the M-cluster of NifDK. Capturing crystallographic snapshots of NifDK structures with substrates being partially reduced at the M-cluster S2B site or completely reduced at M-cluster S5A site would provide direct evidence of the proposed belt-sulfur mobilization mechanism of nitrogenase catalysis. One future experiment could be geared more towards mutating certain amino acid residues such as Histidine 195, which showed distinct substrate reduction activities when having different mutations. Mutating residue 195 could potentially lead to new knowledge about the function of specific belt-sulfur sites.

BIBLIOGRAPHY

Chen, C., Liu, Y., & Yao, Y. (2020). Ammonia Synthesis via Electrochemical Nitrogen Reduction Reaction on Iron Molybdate under Ambient Conditions. *European Journal of Inorganic Chemistry*, *2020*(34), 3236–3241.

Chen, X., & Thibeault, S. (2013). Effect of DMSO Concentration, Cell Density and Needle Gauge on the Viability of Cryopreserved Cells in Three Dimensional Hyaluronan Hydrogel. *Conference Proceedings : ... Annual International Conference of the IEEE Engineering in Medicine and Biology Society. IEEE Engineering in Medicine and Biology Society. Conference*, *2013*, 6228–6231.

Georgiadis, M. M., Komiya, H., Chakrabarti, P., Woo, D., Kornuc, J. J., & Rees, D. C. (1992). Crystallographic Structure of the Nitrogenase Iron Protein from *Azotobacter vinelandii*. *Science*, *257*(5077), 1653–1659.

Global Climate Change: Evidence. (2008, June 15). Retrieved January 14, 2023, from http://climate.nasa.gov/evidence/. (n.d.).

Goldsmith, M., Kiss, C., Bradbury, A. R. M., & Tawfik, D. S. (2007). Avoiding and controlling double transformation artifacts. *Protein Engineering Design and Selection*, *20*(7), 315–318.

González-Cabaleiro, R., Thompson, J. A., & Vilà-Nadal, L. (2021). Looking for Options to Sustainably Fixate Nitrogen. Are Molecular Metal Oxides Catalysts a Viable Avenue? *Frontiers in Chemistry*, *9*, 742565.

Hermann Bothe. (2007). *Biology of the Nitrogen Cycle*. Elsevier.

Hu, Y., Corbett, M. C., Fay, A. W., Webber, J. A., Hedman, B., Hodgson, K. O., & Ribbe, M. W. (2005). Nitrogenase reactivity with P-cluster variants. *Proceedings of the National Academy of Sciences*, *102*(39), 13825–13830.

Hu, Y., Fay, A. W., Lee, C. C., Wiig, J. A., & Ribbe, M. W. (2010). Dual functions of NifEN: Insights into the evolution and mechanism of nitrogenase. *Dalton Transactions (Cambridge, England : 2003)*, *39*(12), 2964–2971.

Hu, Y., Fay, A. W., & Ribbe, M. W. (2007). Molecular insights into nitrogenase FeMo cofactor insertion: The role of His 362 of the MoFe protein α subunit in FeMo cofactor incorporation. *JBIC Journal of Biological Inorganic Chemistry*, *12*(4), 449–460.

Hu, Y., & Ribbe, M. W. (2013a). Biosynthesis of the Iron-Molybdenum Cofactor of Nitrogenase. *Journal of Biological Chemistry*, *288*(19), 13173–13177.

Hu, Y., & Ribbe, M. W. (2013b). Nitrogenase assembly. *Biochimica et Biophysica Acta (BBA) - Bioenergetics*, *1827*(8–9), 1112–1122.

Jasniewski, A. J., Sickerman, N. S., Hu, Y., & Ribbe, M. W. (2018). The Fe Protein: An Unsung Hero of Nitrogenase. *Inorganics*, *6*(1), Article 1.

Jørgensen, S. E., & Fath, B. D. (2008). *Encyclopedia of ecology*. Elsevier.

Kang, W., Lee, C. C., Jasniewski, A. J., Ribbe, M. W., & Hu, Y. (2020). Structural evidence for a dynamic metallocofactor during N_2 reduction by Mo-nitrogenase. *Science*, *368*(6497), 1381–1385.

Kim, J., & Rees, D. C. (1994). Nitrogenase and biological nitrogen fixation. *Biochemistry*, *33*(2), 389–397.

Lanzilotta, W. N., Parker, V. D., & Seefeldt, L. C. (1999). Thermodynamics of nucleotide interactions with the Azotobacter vinelandii nitrogenase iron protein. *Biochimica et Biophysica Acta (BBA) - Protein Structure and Molecular Enzymology*, *1429*(2), 411–421.

Lee, C. C., Blank, M. A., Fay, A. W., Yoshizawa, J. M., Hu, Y., Hodgson, K. O., Hedman, B., & Ribbe, M. W. (2009). Stepwise formation of P-cluster in nitrogenase MoFe protein. *Proceedings of the National Academy of Sciences of the United States of America*, *106*(44), 18474–18478.

Leigh Krietsch Boerner. (2019, June 15). Industrial ammonia production emits more CO2 than any other chemical-making reaction. Chemists want to change that. *Chemical & Engineering News*.

Sickerman, N. S., Hu, Y., & Ribbe, M. W. (2017). Chapter Nine - Nitrogenase Assembly: Strategies and Procedures. In S. S. David (Ed.), *Methods in Enzymology* (Vol. 595, pp. 261–302). Academic Press.

Sickerman, N. S., Rettberg, L. A., Lee, C. C., Hu, Y., & Ribbe, M. W. (2017). Cluster assembly in nitrogenase. *Essays in Biochemistry*, *61*(2), 271–279.

Spatzal, T., Schlesier, J., Burger, E.-M., Sippel, D., Zhang, L., Andrade, S. L. A., Rees, D. C., & Einsle, O. (2016). Nitrogenase FeMoco investigated by spatially resolved anomalous dispersion refinement. *Nature Communications*, *7*(1), 10902.

Structure of a cofactor-deficient nitrogenase MoFe protein. (Reports)—Document—Gale Academic OneFile. (n.d.). Retrieved December 5, 2022, from

Tezcan, F. A., Kaiser, J. T., Howard, J. B., & Rees, D. C. (2015). Structural Evidence for Asymmetrical Nucleotide Interactions in Nitrogenase. *Journal of the American Chemical Society*, *137*(1), 146–149.

CURRICULUM VITAE